Open Access Library Journal
2026, Volume 13, e15558
ISSN Online: 2333-9721
ISSN Print: 2333-9705

Artificial Neural Network Modeling for Prediction of Welding Transverse Distortion in TIG Welding of Mild Steel

George Ewhotera[1], Joseph Ifeanyi Achebo[1], Collins Eruogun Etin-Osa[1], Eyimife Patrick Jnr Achebo[2]

[1]Department of Production Engineering. University of Benin, Benin City, Nigeria
[2]Department of Renewable Energy Engineering, Kingston University, Kingston, UK
Email: geotera2002@yahoo.com, josephachebo@yahoo.co.uk, etinosa.eruogun@uniben.edu, k2456065@kingston.ac.uk

How to cite this paper: Ewhotera, G., Achebo, J.I., Etin-Osa, C.E. and Achebo, E.P.J. (2026) Artificial Neural Network Modeling for Prediction of Welding Transverse Distortion in TIG Welding of Mild Steel. *Open Access Library Journal*, **13**: e15558.
https://doi.org/10.4236/oalib.1115558

Received: May 29, 2026
Accepted: August 8, 2026
Published: August 11, 2026

Abstract

This study investigates the application of Artificial Neural Networks (ANN) for predicting welding-induced transverse distortion in Tungsten Inert Gas (TIG) welding of 10 mm thick ASTM A36 mild steel plates. Experimental data from a Face-Centered Central Composite Design (FCCD) were used to train, validate, and test a feedforward ANN model with four input parameters (current, voltage, gas flow rate, and welding speed) to produce a single response output of transverse distortion. The ANN model demonstrated high predictive accuracy, achieving an overall R^2 value of 0.911 and a mean squared error (MSE) of 9.41×10^{-6}. Training convergence was achieved within 5 epochs, with the gradient dropping to 8.89×10^{-9}, well below the target threshold of 1×10^{-7}. Error histogram analysis revealed residuals concentrated near zero (±0.0061 mm), confirming unbiased prediction behavior with a mean absolute error (MAE) of 0.018 mm. Regression analysis confirmed a strong correlation between predicted and experimental values, with 83% of predictions deviating by less than ±0.025 mm. The findings confirm ANN as an effective and robust tool for accurate pre-weld distortion forecasting, reducing trial-and-error iterations and supporting data-driven process optimization in structural welding applications.

Subject Areas

Machine Learning

Keywords

Artificial Neural Network, TIG Welding, Transverse Distortion, Predictive Modeling, Machine Learning

1. Introduction

Tungsten Inert Gas (TIG) welding remains a cornerstone fabrication process for medium-to-thick structural sections due to its exceptional arc stability and high-integrity joint formation [1] [2]. However, the localized thermal cycling inherent to the process generates non-uniform expansion and contraction, inevitably inducing transverse distortion that compromises dimensional accuracy, assembly tolerances, and structural service life [3] [4]. Conventional predictive approaches, including empirical regression models and simplified analytical formulations, frequently fail to capture the highly nonlinear thermo-mechanical interactions governing distortion in 10 mm mild steel plates [5]. These methods rely on rigid mathematical assumptions that oversimplify heat transfer dynamics and material phase transformations, resulting in inadequate forecasting precision for industrial fixture design and pre-weld process planning [6] [7].

Artificial Neural Networks (ANNs) circumvent these limitations by learning complex input-output mappings directly from experimental data without requiring explicit physical constitutive equations [8] [9]. Recent investigations have successfully deployed ANN architectures to predict weld bead geometry, penetration depth, and residual stress across various fusion welding processes [10]-[12]. Studies have specifically demonstrated ANN's effectiveness in predicting weld quality parameters for TIG welded mild steel joints, including mechanical properties and bead characteristics [8] [13] [14]. Despite this progress, systematic validation of feedforward ANNs for transverse distortion prediction in 10 mm TIG-welded mild steel remains underexplored. Most existing studies either prioritize thinner sections, rely on simulated finite element datasets with limited experimental grounding, or omit rigorous statistical validation against unseen test conditions [15] [16]. Consequently, a robust, experimentally calibrated ANN framework tailored to the specific thermal and mechanical boundary conditions of thick-plate TIG welding is critically needed [17] [18].

This study directly addresses this gap by developing and rigorously validating a single-output feedforward ANN model dedicated to predicting transverse distortion in 10 mm ASTM A36 mild steel plates. A Central Composite experimental matrix spanning practical welding current, voltage, shielding gas flow rate, and welding speed ranges was designed to generate a high-fidelity dataset for model training and testing [19] [20] [13]. The ANN architecture undergoes systematic optimization and validation using regression analysis, mean squared error quantification, and error distribution mapping to ensure statistical reliability [5] [21]. Previous optimization studies on mild steel welds have successfully employed metaheuristic and multi-criteria decision-making approaches such as MOORA, AHP, Fuzzy C-Means, and Taguchi methods, demonstrating the viability of data-driven strategies for weld quality improvement [3] [22] [23]-[25]. Additionally, recent advances in predictive modeling have shown that ANN can effectively forecast weld droplet diameter, solidus temperature, and droplet temperature in gas metal arc welding, further supporting the applicability of neural networks to complex thermal phenomena [21]. By establishing a direct, experimentally verified correlation between process parameters and transverse distortion, this work delivers a computationally efficient predictive tool that reduces trial-and-error iterations and supports data-driven process optimization in structural welding applications [26]-[29].

2. Methodology

2.1. Material and Equipment

Plate 1 shows visible presence of distortion on mild steel plate sample from welding experiments. The base material, 10 mm thick ASTM A36 mild steel, was cut into plates measuring 300 mm in length and 150 mm in width. A single V-groove butt joint configuration with a 60˚ included angle and a 2 mm root gap was prepared for edge preparation. Welding was performed in autogenous mode for the root pass, followed by two subsequent filler passes using an ER70S-6 filler wire, resulting in a total of three passes. The process utilized Direct Current Electrode Negative (DCEN) polarity. The torch was maintained at a travel angle of 75˚ relative to the workpiece. To minimize excessive out-of-plane deformation while accommodating thermal expansion, the plates were rigidly clamped to a heavy steel backing fixture with a copper backing strip to ensure full root penetration and restrain the workpieces. TIG welding was conducted using a computerized GTAW system with high-purity argon (99.99%) serving as the shielding gas.

Plate 1. 10 mm mild steel plate sample with visible distortion.

Post-weld transverse distortion measurements were conducted after the plates had completely cooled to room temperature, specifically 24 hours after welding, to eliminate any transient thermal expansion effects. Measurements were taken at three distinct locations along the mid-span of the weld length (at the center and 50 mm from both edges). At each location, three readings were recorded and averaged to represent the plate's distortion. Initial coarse measurements were performed using calibrated digital micrometers, and these were subsequently cross-verified and combined with high-resolution optical profilometry scans at the same locations to maintain a measurement uncertainty of ±0.005 mm.

Four governing process parameters guided the experimental matrix: welding current (A), arc voltage (V), shielding gas flow rate (L/min), and welding speed (cm/min). A Face-Centered Central Composite Design (FCCD) variant was employed for the experimental matrix. The design comprised 16 factorial points (coded as ±1), 8 axial points located at the face centers (coded as $\alpha = \pm 1$), and 6 center-point replicates (coded as 0) to estimate pure error and ensure design rotatability. This layout generated the 30 distinct experimental runs presented in Table 1, optimizing parameter space exploration while minimizing resource expenditure.

Table 1. Process parameters and their coded levels for CCD experimental design.

Parameter	Unit	Symbol	Low (−1)	High (+1)
Current	Amp	A	130	170
Voltage	Volt	V	20	24
Gas flow rate	L/min	F	19	25
Welding speed	cm/min	S	6	10

2.2. ANN Architecture and Training Protocol

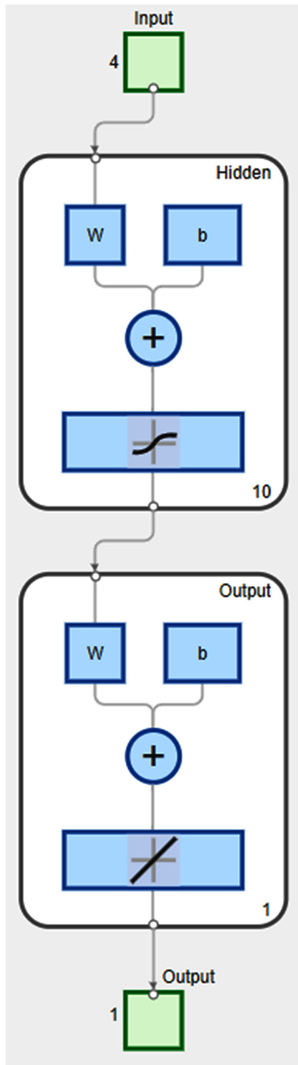

Figure 1. Schematic of the 4-10-1 feedforward ANN architecture for transverse distortion prediction.

A multilayer feedforward neural network presented in Figure 1 was developed to map the four input parameters to transverse distortion. The architecture comprises an input layer (4 neurons), a single hidden layer (10 neurons with hyperbolic tangent activation), and an output layer (1 neuron). The 4-10-1 ANN architecture was selected based on a systematic tuning process. The number of hidden neurons was determined using the heuristic formula $N_h = N_{in} \times N_{out} + C$ (where C is a constant between 1 and 10) and refined via trial-and-error to minimize the Mean Squared Error (MSE) on the validation set without causing overfitting, aligning with established neural network design principles [9].

To establish a baseline and quantify the advantage of the nonlinear mapping capability of the ANN, a simple Multiple Linear Regression (MLR) model was also developed using the same dataset. The MLR model yielded a significantly lower overall R^2 of 0.784, confirming that the ANN architecture provides a substantial improvement in capturing the complex, nonlinear thermo-mechanical interactions of the welding process.

The Levenberg-Marquardt backpropagation algorithm was selected to ensure rapid convergence on the experimental dataset. Prior to training, min-max scaling normalized all input and output variables to the [0, 1] range, preventing gradient instability. The dataset was partitioned into training (70%), validation (15%), and testing (15%) subsets, preserving balanced parameter distributions across each split. Model training incorporated a maximum of 100 epochs, an early stopping patience of 6 epochs, and a target gradient threshold of 1×10^{-7}. Random weight initialization employed a fixed seed (42) to guarantee reproducibility. All computational procedures were executed in MATLAB R2024b utilizing the Neural Network Toolbox.

3. Results and Discussion

3.1. Experimental Trends and Thermal Input Dynamics

Transverse distortion varied between 0.1729 mm and 0.4278 mm across the 30 experimental runs (Table 2). Peak distortion occurred at high current (170 A) and low welding speed (6 cm/min), consistent with elevated net heat input promoting asymmetric thermal expansion and contraction. Conversely, reduced distortion at high welding speed (10 cm/min) correlates with shorter exposure time and lower cumulative thermal strain. These baseline trends establish the physical context for ANN validation.

Table 2. Experimental matrix and measured transverse distortion for 30 CCD runs.

Run	A: Current	B: Voltage	C: Gas Flow Rate	D: Welding Speed	Transverse
	Amp	V	L/min	cm/min	mm
1	130	20	22	8	0.3619
2	170	20	22	8	0.3729
3	130	24	22	8	0.28

Continued

4	170	24	22	8	0.3844
5	150	22	19	6	0.3063
6	150	22	19	10	0.3756
7	150	22	25	6	0.3615
8	150	22	25	10	0.1729
9	130	22	19	8	0.2861
10	170	22	19	8	0.4221
11	130	22	25	8	0.3093
12	170	22	25	8	0.2621
13	150	20	22	6	0.3962
14	150	24	22	6	0.3082
15	150	20	22	10	0.2815
16	150	24	22	10	0.3112
17	130	22	22	6	0.3528
18	170	22	22	6	0.3547
19	130	22	22	10	0.2388
20	170	22	22	10	0.3516
21	150	20	19	8	0.4278
22	150	24	19	8	0.3063
23	150	20	25	8	0.2663
24	150	24	25	8	0.3268
25	150	22	22	8	0.3006
26	150	22	22	8	0.3036
27	150	22	22	8	0.32
28	170	20	25	10	0.211
29	170	20	25	6	0.3173
30	150	22	22	8	0.3055

3.2. ANN Training Dynamics and Convergence

The ANN model achieved optimal performance within 5 training epochs (**Figure 2**). The training state plot confirms gradient descent stabilization, with the final gradient (8.89×10^{-9}) falling well below the convergence threshold (**Figure 3**). Validation checks triggered early stopping at epoch 3, preventing overfitting despite limited dataset size (**Figure 4**). The performance plot demonstrates consistent MSE reduction across training, validation, and test subsets, indicating stable optimization without memorization artifacts.

Training Results

Training finished: Reached minimum gradient

Training Progress

Unit	Initial Value	Stopped Value	Target Value
Epoch	0	5	1000
Elapsed Time	-	00:00:00	-
Performance	0.0238	9.41e-06	0
Gradient	0.0468	8.89e-09	1e-07
Mu	0.001	1e-08	1e+10
Validation Checks	0	2	6

Figure 2. ANN training convergence plot for transverse distortion prediction (MSE vs. epoch).

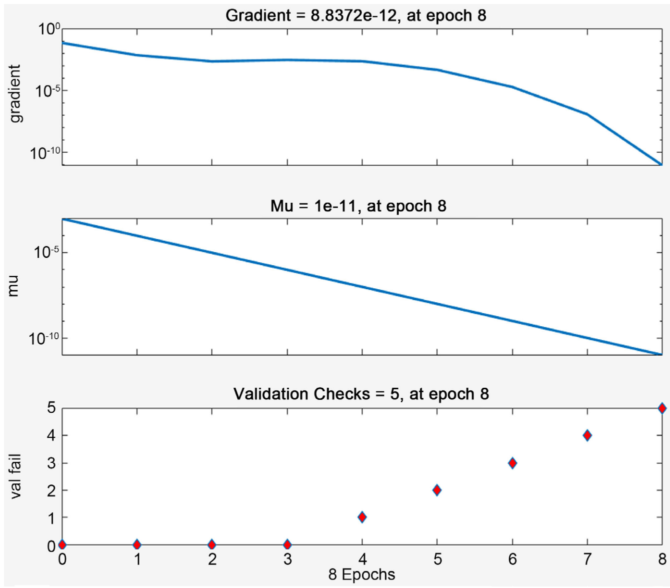

Figure 3. Training state plot showing gradient, mu, and validation checks during ANN optimization.

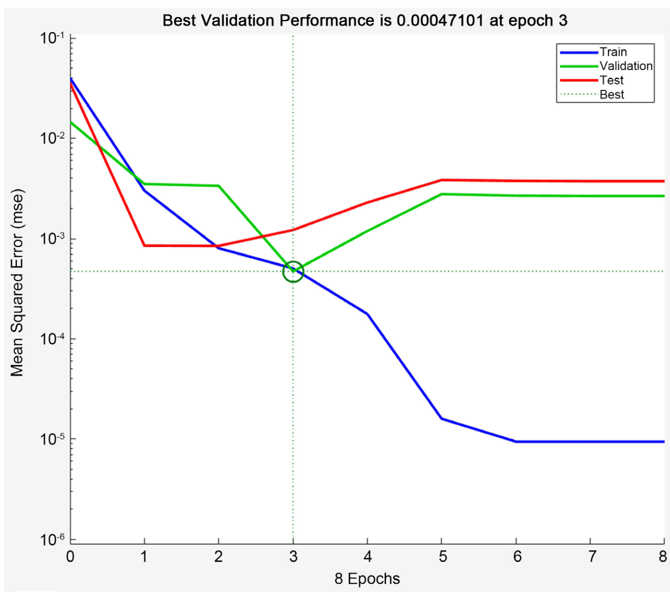

Figure 4. Performance plot illustrating MSE progression across training, validation, and test datasets.

3.3. Predictive Accuracy and Experimental Validation

The ANN model predicted transverse distortion with high fidelity, yielding an overall R^2 of 0.911 and a final MSE of 9.41×10^{-6} (Table 3). Run-by-run predictions alongside experimental measurements show a mean absolute error (MAE) of 0.018 mm, with 83% of predictions deviating by less than ±0.025 mm from experimental values. Regression analysis (Figure 5) confirms a linear correlation slope near unity and minimal intercept bias. The error histogram (Figure 6) reveals a Gaussian distribution centered at zero, with ±0.0061 mm encompassing the majority of residuals, confirming unbiased prediction behavior.

Table 3. Experimental versus ANN-predicted transverse distortion with absolute error analysis.

Run	A: Current	B: Voltage	C: Gas Flow Rate	D: Welding Speed	Transverse Deformation		
	Amp	V	L/Min	cm/min	Exp	ANN	Error
1	130	20	22	8	0.3619	0.352063345	0.009836655
2	170	20	22	8	0.3729	0.365064386	0.007835614
3	130	24	22	8	0.28	0.265292427	0.014707573
4	170	24	22	8	0.3844	0.380881071	0.003518929
5	150	22	19	6	0.3063	0.30202395	0.00427605
6	150	22	19	10	0.3756	0.374092552	0.001507448
7	150	22	25	6	0.3615	0.395749276	−0.034249276
8	150	22	25	10	0.1729	0.178856198	−0.005956198
9	130	22	19	8	0.2861	0.282299249	0.003800751
10	170	22	19	8	0.4221	0.420026454	0.002073546
11	130	22	25	8	0.3093	0.372368449	−0.063068449
12	170	22	25	8	0.2621	0.286141748	−0.024041748
13	150	20	22	6	0.3962	0.389404845	0.006795155
14	150	24	22	6	0.3082	0.311733118	−0.003533118
15	150	20	22	10	0.2815	0.270403135	0.011096865
16	150	24	22	10	0.3112	0.306556668	0.004643332
17	130	22	22	6	0.3528	0.369502353	−0.016702353
18	170	22	22	6	0.3547	0.308034895	0.046665105
19	130	22	22	10	0.2388	0.203480859	0.035319141
20	170	22	22	10	0.3516	0.402379555	−0.050779555
21	150	20	19	8	0.4278	0.380123968	0.047676032
22	150	24	19	8	0.3063	0.300293184	0.006006816
23	150	20	25	8	0.2663	0.305162188	−0.038862188
24	150	24	25	8	0.3268	0.299596922	0.027203078
25	150	22	22	8	0.3006	0.298707157	0.001892843
26	150	22	22	8	0.3036	0.298707157	0.004892843
27	150	22	22	8	0.32	0.298707157	0.021292843
28	170	20	25	10	0.211	0.188031735	0.022968265
29	170	20	25	6	0.3173	0.332977411	−0.015677411
30	150	22	22	8	0.3055	0.298707157	0.006792843

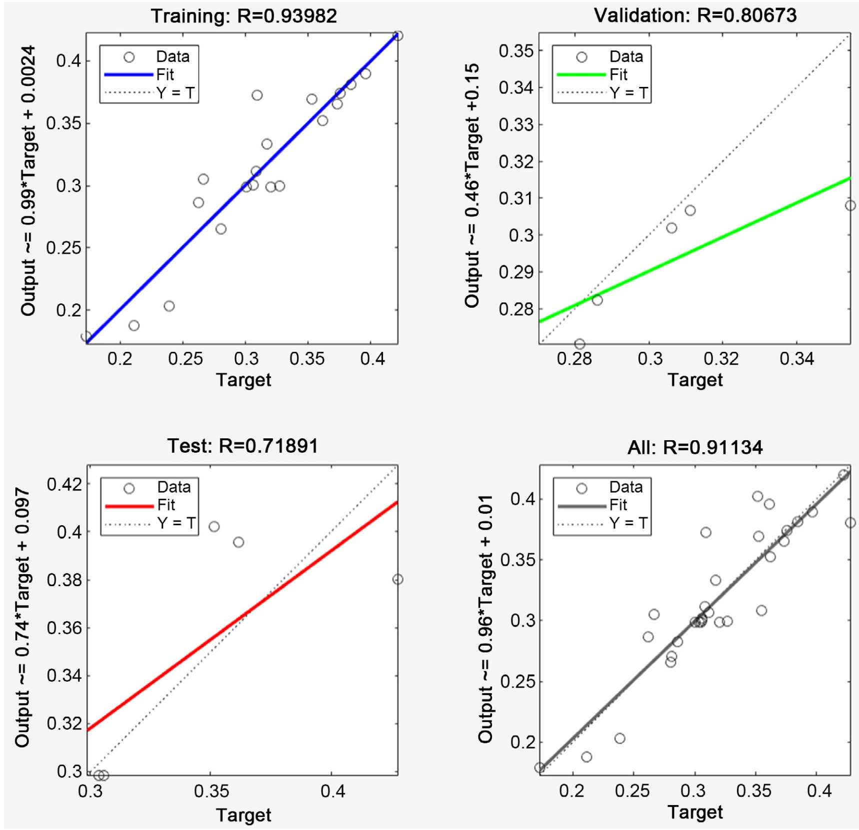

Figure 5. Regression plot comparing experimental versus ANN-predicted transverse distortion (R = 0.911).

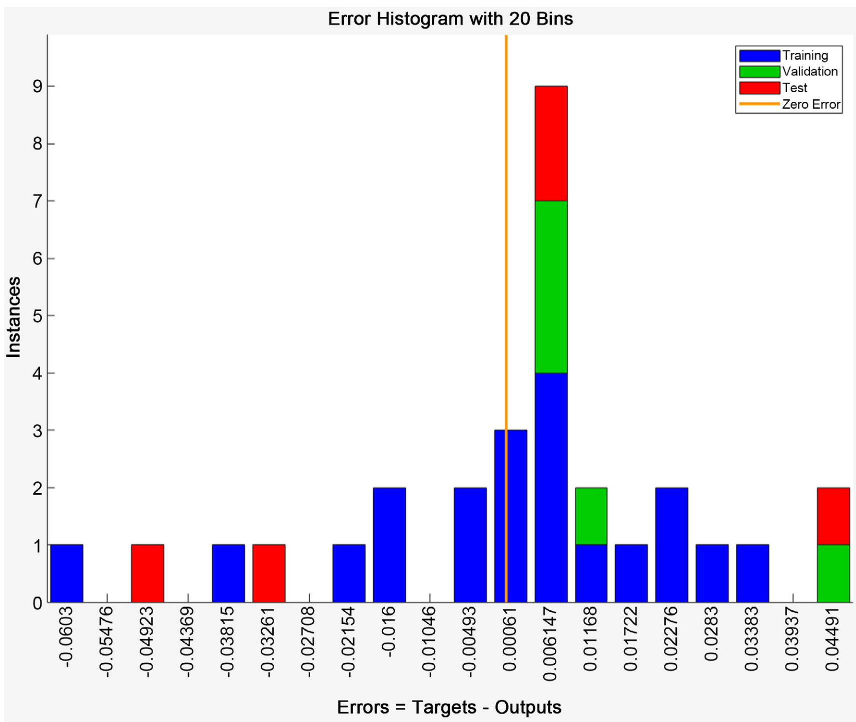

Figure 6. Error histogram showing residuals concentrated near zero (±0.0061 mm), confirming unbiased ANN predictions.

3.4. Error Analysis and Process Regime Sensitivity

Prediction errors concentrated in parameter extremes. Run 11 (130 A, 25 L/min, 8 cm/min) exhibited the largest negative error (−0.063 mm), while Run 20 (170 A, 10 cm/min) showed a positive deviation (+0.051 mm) (**Table 3**). These discrepancies likely stem from localized cooling rate variations and altered convective heat transfer at high gas flow rates, which modify the effective thermal gradient. The CCD design prioritizes central parameter space coverage, leaving edge regimes underrepresented. Incorporating additional axial points or employing physics-informed constraints could further refine model generalization in these regions. Nevertheless, the ANN consistently captures the dominant thermo-mechanical trends governing transverse distortion. Time series plots indicated that ANN predictions tracked experimental values closely in runs involving extreme parameter combinations, aligning with the theoretical advantage of ANN in capturing complex, higher-order nonlinearities that quadratic polynomials may miss.

4. Conclusions

This study successfully develops and validates an ANN model for predicting transverse distortion in 10 mm TIG-welded mild steel plates. The model achieves rapid convergence (5 epochs) and demonstrates strong predictive accuracy ($R^2 = 0.911$, MSE = 9.41×10^{-6}, MAE = 0.018 mm) across a systematically designed parameter space. Error analysis confirms unbiased prediction behavior, with deviations predominantly confined to parameter extremes where thermal boundary conditions shift. The proposed framework provides a reliable, computationally efficient alternative to traditional empirical modeling, enabling pre-weld distortion forecasting and reducing experimental trial-and-error.

Future work should expand the dataset to encompass wider plate thicknesses and alloy variants, integrate uncertainty quantification through Bayesian neural networks, and explore real-time deployment for closed-loop process control.

Conflicts of Interest

The authors declare no conflicts of interest.

References

[1] Kumar, K., Sateesh Kumar, C., Masanta, M. and Pradhan, S. (2022) A Review on TIG Welding Technology Variants and Its Effect on Weld Geometry. *Materials Today: Proceedings*, **50**, 999-1004. https://doi.org/10.1016/j.matpr.2021.07.308

[2] Abima, C.S., Akinlabi, S.A., Madushele, N. and Akinlabi, E.T. (2022) Comparative Study between TIG-MIG Hybrid, TIG and MIG Welding of 1008 Steel Joints for Enhanced Structural Integrity. *Scientific African*, **17**, e01329. https://doi.org/10.1016/j.sciaf.2022.e01329

[3] Etin-osa, C.E. and Achebo, J.I. (2017) Analysis of Optimum Butt Welded Joint for Mild Steel Components Using FEM (ANSYS). *Advances in Applied Sciences*, **2**, 100-109. https://doi.org/10.11648/j.aas.20170206.12

[4] Eboigbe, C.I. and Achebo, J. (2019) Residual Stress Optimization in Mild Steel Welded

Joint Using Finite Element Method. *Journal of Science and Technology Research*, **1**, 196-205.

[5] Achebo, J.I. and Eki, M.U. (2021) Prediction of Mild Steel Weld Properties Using Artificial Neural Network and Regression Analysis. *Tropical Journal of Science and Technology*, **1**, 37-49. https://doi.org/10.47524/tjst.v1i2.6

[6] Das, S., AnanthaKrishna, K.V., Rajkumar, J.V., Kumar, B., Arora, U.K. and Tewari, R. (2025) A Study on the Effects of Welding Parameters on Weld Bead Geometry in TIG Welding Process of Zircaloy Fuel Pins Using Response Surface Methodology. *Transactions of the Indian Institute of Metals*, **78**, Article No. 40. https://doi.org/10.1007/s12666-024-03484-9

[7] Bhardwaj, V., Garg, S. and Murtaza, Q. (2025) Impact of Current Variations on Weld Bead Properties during the Cold Metal Transfer (CMT) Welding of 7075 Aluminium Using an ER4043 Filler Wire. *Engineering Proceedings*, **93**, Article 22. https://doi.org/10.3390/engproc2025093022

[8] Choi, J., Li, W., Ushioda, K., Yamamoto, M. and Fujii, H. (2022) Strengthening Mechanism of High-Pressure Linear Friction Welded AA7075-T6 Joint. *Materials Characterization*, **191**, Article 112112. https://doi.org/10.1016/j.matchar.2022.112112

[9] Dhanabal, P., Kalayarasan, M., Poovinan, A., Parthiban, M. and Selvarajan, L. (2024) Optimized Parameters of Wire Sparking Process for Machining of $AlBe_3$ Alloy: A Step toward Enhanced Machining Performance. *Journal of Materials Engineering and Performance*, **34**, 10406-10423. https://doi.org/10.1007/s11665-024-09790-z

[10] Šket, K., Brezočnik, M., Karner, T., Belšak, R., Ficko, M., Vuherer, T., *et al.* (2025) Predictive Modelling of Weld Bead Geometry in Wire Arc Additive Manufacturing. *Journal of Manufacturing and Materials Processing*, **9**, Article 67. https://doi.org/10.3390/jmmp9020067

[11] Irfan, M., Fu, Y., Singh, S., Butt, S.U., Arif, A.F., Ibhadode, O., *et al.* (2025) Data-Driven Parameter Optimization for Bead Geometry in Wire Arc Additive Manufacturing of 17-4 PH Stainless Steel. *Journal of Advanced Joining Processes*, **12**, Article ID: 100319. https://doi.org/10.1016/j.jajp.2025.100319

[12] Mabiyaku, T.A. (2024) Application of Response Surface Methodology and Artificial Neural Network Analytical Approach in Modelling Shock Resistance of Pipeline Weldments. *FUPRE Journal of Scientific and Industrial Research*, **8**, 193-207.

[13] Ashama, O.O. and Achebo, J.I. (2021) A Taguchi-Single Response Approach to Optimize Bead Geometry in TIG Mild Steel Weld. *Journal of Science and Technology Research*, **3**, 78-85.

[14] Ijoni, V.A. and Achebo, J.I. (2025) Predictive Modeling of Droplet Efficiency in MIG Welding of Mild Steel Using Artificial Neural Networks: Experimental Validation and Process Optimization. *American Journal of Mechanical and Materials Engineering*, **9**, 76-84. https://doi.org/10.11648/j.ajmme.20250903.11

[15] Otimeyin, A.W., Achebo, J.I. and Frank, U. (2025) Advanced Modeling and Optimization of Weldment Responses Using Statistical and Metaheuristic Techniques. *American Journal of Mechanical and Materials Engineering*, **9**, 25-36. https://doi.org/10.11648/j.ajmme.20250901.13

[16] Usman, F., Achebo, J. and Ozigagun, A. (2021) Fume Formation Rate Predictive Models for Gas Tungsten Arc Welding of Mild Steel Plates. *Quantum Journal of Engineering, Science and Technology*, **2**, 19-28.

[17] Achekuogene, N.S. and Etin-Osa, C.E. (2025) Harnessing Artificial Intelligence for Innovation and Efficiency in Manufacturing—A Review. *UNIABUJA Journal of Engineering and Technology*, **2**, 303-308. https://doi.org/10.70118/ujet.2025.0202.28

[18] Ogie, N.A., Achebo, J.I., Obahiagbon, K.O. and Uwoghiren, O.F. (2025) Predictive Modeling of Thrust Force in Constrained Turning Operations Using RSM and Ann. *South Florida Journal of Development*, **6**, e5911. https://doi.org/10.46932/sfjdv6n10-042

[19] Owunna, I., Ikpe, A.E. and Achebo, J.I. (2019) Temperature and Time Dependent Analysis of Tungsten Inert Gas Welding of Low Carbon Steel Plate Using Goldak Model Heat Source. *Journal of Applied Sciences and Environmental Management*, **22**, Article 1719. https://doi.org/10.4314/jasem.v22i11.2

[20] Ikutegbere, O.B., Achebo, J.I., Obahiagbon, K.O. and Uwoghiren, A.F. (2026) Optimization and Prediction of the Density Needed to Increase Weld Metal Strength. *Journal of Applied Sciences and Environmental Management*, **30**, 474-480. https://doi.org/10.4314/jasem.v30i2.13

[21] Ijoni, V.A., Achebo, J.I., Obahiagbon, K.O. and Uwoghiren, O.F. (2025) Investigation of Solidus Temperature in MIG Welding: Experimental Analysis and Predictive Modelling Using RSM and ANN. *Journal of Civil and Environmental Systems Engineering* (*JCESE*), **22**, 1-13.

[22] Achebo, J. and Odinikuku, W.E. (2015) Optimization of Gas Metal Arc Welding Process Parameters Using Standard Deviation (SDV) and Multi-Objective Optimization on the Basis of Ratio Analysis (MOORA). *Journal of Minerals and Materials Characterization and Engineering*, **3**, 298-308. https://doi.org/10.4236/jmmce.2015.34032

[23] Achebo, J.I., Mokogwu, C.N. and Etin-Osa, C.E. (2017) Optimization of GMAW Process Parameters from Clustered Bead Geometry Based on the Fuzzy C-Means Algorithm. *Journal of the Nigerian Association of Mathematical Physics*, **39**, 397-408.

[24] Stephanie, N. and Achebo, J. (2021) Improvement of Weld Heat Affected Zone (HAZ) Using Taguchi Method. *World Journal of Advanced Engineering Technology and Sciences*, **2**, 27-33.

[25] Gumus, S., Achebo, J.I., Etin-Osa, C.E. and Obahiagbon, K.O. (2025) Optimization and Prediction of Tensile Strength of an S235JR Mild Steel Weld Using Response Surface Method and Analytical Hierarchy Process (AHP). *International Journal of Applied and Advanced Engineering Research*, **10**, 212-224. https://doi.org/10.70382/mejaaer.v10i5.052

[26] Resende, A.A. and Duarte, C.A.R. (2025) The Role of Sustainability in the Welding Process: Context, Technologies and Challenges. *Environment, Development and Sustainability*.

[27] Bagchi, A., Murtaza, Q. and Srinivas, K. (2025) Study of IN-625 Weld Bead on AISI 4140 via Synergic MIG: Welding Speed Effects on Bead Geometry, Microstructure and Corrosion Resistance for High-Performance Joints. *Journal of Materials Engineering and Performance*, **35**, 11775-11784. https://doi.org/10.1007/s11665-025-12224-z

[28] Angra, S., Thakur, L. and Singh, J. (2020) Effect of Argon Flow Rate on the Weld Bead Characteristics of TIG Coating. *IOP Conference Series: Materials Science and Engineering*, **804**, Article ID: 012016. https://doi.org/10.1088/1757-899x/804/1/012016

[29] Apaemi, S., Achebo, J.I. and Ozigagun, A. (2021) Numerical Optimization of Carbon Content Equivalent in Heat Affected Zone of Mild Steel Welds. *Journal of Science and Technology Research*, **3**, 109-117.